JOURNAL OF PETROLOGY | PAGES 1 of 19 | doi:10.1093/petrology/egh043

Journal of Petrology Advance Access published August 19, 2004

The Significance of Multiple Saturation Points in the Context of Polybaric Near-fractional Melting

PAUL D. ASIMOW[1]* AND JOHN LONGHI[2]

[1]DIVISION OF GEOLOGICAL AND PLANETARY SCIENCES 170-25, CALIFORNIA INSTITUTE OF TECHNOLOGY, PASADENA, CA 91125, USA

[2]LAMONT–DOHERTY EARTH OBSERVATORY, PALISADES, NY 10964, USA

RECEIVED JULY 2, 2003; ACCEPTED APRIL 6, 2004

Experimental petrologists have successfully located basaltic liquid compositions parental to mid-ocean ridge basalt that are, within experimental resolution, multiply saturated with three-phase harzburgite or four-phase lherzolite assemblages on their liquidus at some elevated pressure. Such an experimental result is a necessary consequence of any paradigm in which erupted basalts derive from single-batch primary liquids that equilibrate with a mantle residue and undergo no subsequent magma mixing before differentiation and eruption. Here we investigate whether, conversely, such evidence of multiple saturation is sufficient to exclude dynamic melting models wherein increments of melt are mixed after segregation from residues, during melt transport or in magma chambers. Using two independent models of crystal–liquid equilibria to simulate polybaric near-fractional peridotite melting, we find that aggregate liquids from such melting processes can display near-intersections of liquidus surfaces too close to distinguish experimentally from exact multiple saturation points. Given uncertainties in glass compositions, fractionation corrections, experimental temperature and pressure conditions, and achievement of equilibrium, these results suggest that polybaric mixtures can in fact masquerade as mantle-equilibrated single-batch primary liquids. Multiple saturation points on the liquidus surfaces of primitive basalts do, however, preserve information about the average pressure of extraction of their constituent increments of liquid.

KEY WORDS: *mantle melting; basaltic volcanism; experimental igneous petrology; thermodynamic modelling; inverse method*

INTRODUCTION

In the first decades after it became firmly established that basalts in general (Verhoogen, 1954; Kuno, 1959; Yoder & Tilley, 1962) and mid-ocean ridge basalts (MORB) in particular (Engel *et al.*, 1965) are the products of partial fusion of mantle peridotite [as originally postulated by Bowen (1928)], it was generally assumed that the chemical evolution leading to an erupted lava could be simply divided into a melting process and a fractionation process (e.g. O'Hara, 1965; Green & Ringwood, 1967). Physically these processes might be separated by a transport process, but chemically the end product of the melting process was thought of as a well-defined primary melt that must have been in equilibrium with an assemblage of residual mantle minerals before fractionation began.

This paradigm motivated experimental petrologists to hope that post-melting modifications had failed, at least in some cases, to erase evidence of the conditions of melting and to apply the 'inverse method' (BVSP, 1981) to the problem of basalt petrogenesis; that is, to locate the pressures, temperatures, and residual mineral assemblages from which basalts are derived by seeking multiple saturation points on the liquidus surfaces of the most primitive measured glass compositions or their computed more-primitive parental liquids. In some cases, this search was apparently successful. Kushiro & Thompson (1972) found that a primitive olivine tholeiite with Mg-number [molar $100 \times MgO/(MgO + FeO)$] = 64 from the Mid-Atlantic Ridge crystallized olivine, orthopyroxene (opx), clinopyroxene (cpx), and plagioclase within 10°C of one another at 0·75 GPa. Fujii & Kushiro (1977) obtained a similar result on a sample from DSDP site 45, although this sample, with Mg-number = 57,

*Corresponding author. Telephone: (626)395-4133. Fax: (626)568-0935. E-mail: Asimow@gps.caltech.edu

crystallizes olivine with Mg-number = 86 and would now be considered too evolved to be primary. Bender *et al.* (1978) examined a primitive (Mg-number = 68) olivine tholeiite from the FAMOUS area of the Mid-Atlantic Ridge and, although they had only a single opx-bearing experiment at 1·5 GPa, inferred a three-phase olivine–opx–cpx multiple saturation point at 1·05 GPa. Although Green *et al.* (1979) found that the DSDP site 3 sample they studied did not have orthopyroxene near the liquidus under any conditions, they determined that a possible parental composition constructed by mixing the measured sample with 17% olivine produced a liquid that crystallized olivine and then orthopyroxene within 20°C at 2·0 GPa. They concluded from this that they might have identified a primary parental composition in equilibrium with a harzburgite residue at this pressure. We should note that a critical review of these experiments by Falloon & Green (1987) found them all questionable in one way or another as evidence that primitive MORBs are primary melts.

Some very primitive glass compositions have been found in transform domains along the East Pacific Rise, such as the Siqueiros Transform (Perfit *et al.*, 1996). Liquidus experiments on some of these samples show multiple saturation with olivine, opx, cpx, and possibly spinel at 1·2–1·3 GPa (Wendlandt & Ridley, 1994). These samples are distinctive also in lacking the ^{230}Th excess that characterizes most young MORB lavas; they appear to be derived entirely from the relatively shallow spinel peridotite field (Lundstrom *et al.*, 2000). Although it is difficult to argue that these samples represent compositions parental to typical axial MORB, they do exist and could plausibly represent examples of true primary single-batch mantle melts.

The results of these multiple saturation searches, together with thinking based on 'forward method' direct peridotite melting experiments and comparison of compositions using a variety of projection schemes, contributed to the lengthy and ultimately inconclusive debate among those favouring a nearly primary role for the most primitive observed MORBs, formed by equilibration with lherzolite at relatively low pressure near 1 GPa (Presnall *et al.*, 1979; Presnall & Hoover, 1987), and those favouring extensive fractionation from picritic primary liquids formed by high-degree melting leaving a harzburgite residue near 3 GPa (O'Hara, 1965, 1968; Stolper, 1980).

Modern ideas of basalt petrogenesis, however, influenced by physical reasoning about the melting environment (McKenzie, 1984, 1985*b*) as well as a variety of geochemical arguments (Johnson *et al.*, 1990; Johnson & Dick, 1992; Langmuir *et al.*, 1992; Qin, 1993; McKenzie, 1985*a*), postulate a process approximated by polybaric near-fractional melting along an adiabatic path. In its simplest form, this model supposes that increments of liquid are separated from residues over a range of pressures and then transported and mixed without further equilibration with mantle minerals (e.g. Klein & Langmuir, 1987; McKenzie & O'Nions, 1991). More physically plausible refinements of the model call for porous flow of buoyant liquids through interconnected porosity that leads to effective separation of migrating liquids from lherzolitic or harzburgitic assemblages; for example, by formation of replacive dunite in migration channels (Aharonov *et al.*, 1995; Kelemen *et al.*, 1995, 1997). The details of U-series disequilibria (Lundstrom, 2000; Lundstrom *et al.*, 2000) and major- and trace-element chemistry of abyssal peridotites (Asimow, 1999) imply that at least two scales of porosity (i.e. high-flux channels and low-permeability interchannel flow) or a continuum of channel sizes are needed for a full description of the melt migration network. Whatever the details, such scenarios, if true, defy our ability to produce a meaningful primary basalt in a single forward-method experiment. Primary basalts in the traditional sense do not exist in these models; there are only aggregate primary liquids. In fact, the complexity of the model that now exists in the mind of the mantle petrologist has rendered moot the question of whether a multiply saturated experimental liquid can be found that is parental to primitive MORB glasses.

In addition to the problem of mixing after separation from the residue, there is also the possibility that extensive crystal fractionation at mantle or crustal depths, before or after mixing of magmas, may have erased evidence of equilibration with residues from all sampled basalts. Grove *et al.* (1992), for example, documented several samples showing multiple saturation with olivine, plagioclase, and clinopyroxene at 0·8 GPa and inferred a history of high-pressure fractionation even for very primitive samples. Examination of phenocryst assemblages led Grove *et al.* (1992) to further propose a complex scenario in which some fractionation precedes mixing.

Yet, despite the general acceptance of polybaric scenarios for MORB origin and the likelihood of complex fractionation and mixing histories, the observations remain that some liquids apparently parental to primitive MORB do seem to be multiply saturated with mantle assemblages or nearly so. If primitive MORB liquids are really mixtures of liquids last equilibrated with mantle assemblages over a considerable range of conditions, then what is the significance of these observations? Is it possible that these multiple saturation points appear (to within experimental resolution) in polybaric mixed liquids by coincidence or for an as yet unknown systematic reason? The alternative is that the inverse method does in fact provide a strong constraint on petrogenesis and that intersection of more than two liquidus curves requires true equilibration at the multiple saturation point. If this is the case then we must either question the particular record of inverse method experimental

observations on primitive MORB or question some aspect of the currently favoured melt generation scenario, such as the idea of disequilibrium transport.

The physical and thermodynamic processes thought to be involved in generating a primary aggregate liquid are too complex to simulate experimentally, but they can be reproduced instead by manipulation of computer models that are calibrated with the results of many experiments. We apply two such models in this work. First, the self-consistent thermodynamic approach based on the MELTS (Ghiorso & Sack, 1995) or pMELTS (Ghiorso *et al.*, 2002) models conserves both mass and energy while rapidly computing equilibria that capture many notable aspects of peridotite melting and basalt formation. The successes and failures of MELTS as a tool for modelling basalt genesis have been explored at some length in previous studies (Baker *et al.*, 1995; Hirschmann *et al.*, 1998*b*, 1999*a*, 1999*b*; Asimow *et al.*, 2001, 2004). Ghiorso *et al.* (2002) offered a comparison of the new pMELTS calibration with experimental peridotite melting, and selected further comparisons with experiments and with natural basalt compositions are given below. The second model is an empirical approach called MAGPOX that predicts melting paths based on parameterizations of liquidus relations and partition coefficients developed by Longhi (1991, 1992, 2002).

In this paper we use pMELTS and MAGPOX to construct forward models of various mantle melting and melt-transport scenarios, leading to calculated primary or aggregate primary melt compositions. Then, using the same model in each case for consistency, we calculate the liquidus relations of these compositions much as an experimentalist applying the inverse method would do. This combination of forward and inverse models lets us test hypotheses and examine, at least in the context of calibrated model space, the strength of constraints from experimental multiple saturation points. We find, in general, that an extraordinarily close approach to multiple saturation arises on the liquidus of the aggregate primary liquid compositions. Although these aggregate primary liquids were never equilibrated with mantle assemblages after mixing, in fact the approximate multiple saturation points that result do give good estimates of the average pressure from which the liquid increments in the mixtures were extracted. We discuss the significance of these model results for basalt genesis in general and MORB interpretation in particular.

METHOD

pMELTS calculations

The thermodynamic basis of pMELTS, its calibration, and its reliability as a model of peridotite melting have been described by Ghiorso *et al.* (2002), who compared pMELTS predictions with the experiments of Baker & Stolper (1994), Baker *et al.* (1995), Walter (1998) and Falloon *et al.* (1999). However, because pMELTS has not previously been applied to calculations of MORB genesis except in studies of wet melting near hotspots (Asimow & Langmuir, 2003; Asimow *et al.*, 2004), we show here some simple tests of the model against experimental peridotite data and natural MORB compositions. Because we will use a 1 GPa, 1350°C batch melting calculation below, a direct comparison at equal melt fraction is given in Table 1 between pMELTS liquid compositions and liquid compositions from 1 GPa peridotite melting experiments near 1350°C (Falloon & Green, 1987; Hirose & Kushiro, 1993; Hirschmann *et al.*, 1998*a*; Schwab & Johnston, 2001). In each case the nominal bulk composition of the experimental mix was input to pMELTS at 1 GPa pressure and the carbon–carbon monoxide (CCO) oxygen buffer. Temperature was varied until the extent of melting by mass reproduced the value found by mass balance estimates in the experiments; in one case a lower melt fraction was chosen for comparison so that both the experiment and the model equilibrium would have cpx in the residue. Obtaining equal melt fraction between the experiment and pMELTS requires a model temperature 20–40°C higher than the experimental temperature, except for the data of Schwab & Johnston (2001), which require an offset of 80°C; this temperature error is generally much smaller than was required to match melt fractions with the original MELTS calibration (Baker *et al.*, 1995; Hirschmann *et al.*, 1998*b*; Ghiorso *et al.*, 2002). When compared at equal melt fraction, pMELTS does a good job predicting most oxide concentrations in the melt, although Cr_2O_3 is systematically too low and there is a serious error in MnO partitioning. The most serious discrepancy is in Fe–Mg partitioning. At reducing oxygen fugacity conditions comparable with the experiments, pMELTS gives an Mg-number 2–3% too high in the melt and/or an olivine–liquid Fe–Mg exchange K_D systematically higher than expected. This is at least partly the result of the temperature error, as higher temperature favours Mg in the melt. However, the calculations that follow were run under more oxidizing conditions, where the K_D predictions are closer to accepted values (Herzberg & O'Hara, 2002). We show below that, despite these shortcomings, a polybaric melting model using pMELTS does produce plausible primitive MORB compositions, but for the specific purposes of this paper we argue that the absolute accuracy of pMELTS is not at issue. It serves here as a framework where we can simulate processes too complex for direct experimentation and show what is possible in an internally self-consistent construction. As thermodynamic models improve in accuracy, it will be important to revisit this type of calculation and see if the results persist.

Table 1: Comparison of pMELTS with selected experiments at 1 GPa

	1		2		3		4	
Source:	MPY-90		MM3		KLB-1		INT-A	
	Exp	pMELTS	Exp	pMELTS	Exp	pMELTS	Exp	pMELTS
T (°C)	1350	1360	1330	1373	1350	1371	1330	1410
F (%)	24	20·7*	18	18·0	20	20·0	12·2	12·2
SiO_2	49·89	50·33	49·7	50·52	50·67	50·33	50·68	51·75
TiO_2	0·87	0·69	0·48	0·48	0·42	0·71	0·15	0·15
Al_2O_3	15·81	15·47	15·2	14·60	14·61	14·47	12·27	11·69
Cr_2O_3	0·19	0·14	0·24	0·17	0·28	0·16	1·06	0·19
FeO*	6·51	6·13	6·7	6·19	7·64	6·79	6·49	6·57
MgO	12·87	13·17	13·0	13·83	13·39	13·45	15·03	15·19
MnO	0·14	0·01	0·13	0·01	0·13	0·01	0·12	0·02
CaO	11·60	12·14	12·6	12·54	11·17	12·49	13·65	13·50
Na_2O	2·29	1·89	1·6	1·65	1·50	1·46	0·62	0·75
K_2O	—	—	—	—	0·19	0·10	0·17	0·16
Mg-no.	77·3	79·2	76·8	79·9	75·8	77·9	80·5	80·4
K_D	0·333	0·376	0·32	0·376	0·31	0·365	0·352	0·376

All experiments conducted in graphite inner capsules; calculations at CCO buffer. 1, Falloon & Green (1987); 2, Baker *et al.* (1995), reanalysed by Hirschmann *et al.* (1998*a*); 3, Hirose & Kushiro (1993); 4, Schwab & Johnston (2001).
*Lower F chosen for comparison to keep residual cpx in the calculation.

The method for computing polybaric fractional or near-fractional melting along adiabatic paths and for integrating these liquids to obtain model primary aggregate liquids for mid-ocean ridge melting regimes has been illustrated in detail by Asimow *et al.* (2001). Each model case is defined by a source composition and by a potential temperature. Potential temperature is obtained from a metastable liquid-absent equilibrium calculation with the source composition at 1 bar pressure and constrained entropy. To obtain a polybaric aggregate melt, the source peridotite composition begins at high pressure and is decompressed at constant entropy until it intersects its solidus. Thereafter, all the liquid produced in each 0·01 GPa increment of decompression is extracted and the entropy of the residue used as the reference for the next step. This continues to a depth corresponding to the base of the resulting igneous crust. The increments of liquid are integrated using a formalism appropriate for calculating the net magmatic output of a two-dimensional passive flow regime (McKenzie & Bickle, 1988; Plank & Langmuir, 1992; Asimow *et al.*, 2001). For the purposes of comparison with natural basalt data, the resulting primary aggregate liquid can be subjected to isobaric fractional crystallization at 50 MPa pressure and one log unit below the quartz–fayalite–magnetite (QFM) buffer using the original MELTS calibration, which is more accurate than pMELTS at low pressure. We show in Fig. 1 that, applying this method, pMELTS generates plausible parental liquids that can fractionate to generate the observed array of MORB compositions. Figure 1 shows the compositions of published glass analyses from the East Pacific Rise (from petdb.ldeo.columbia.edu, Lehnert *et al.*, 2000) together with liquid lines of descent calculated for aggregate primary melts generated at three potential temperatures (1329°C, 1352°C, and 1377°C) with a slightly depleted source composition (Table 2). The MgO contents of these melts (13–15%) are somewhat higher than is generally inferred for primitive MORB melts (10–13%, Herzberg & O'Hara, 2002), but we have seen that pMELTS errs in predicting anomalously high MgO contents relative to experiments; in any case, a small amount of olivine fractionation reduces this MgO content quickly with relatively little effect on any other oxide. The liquid lines of descent calculated for primary aggregate melts from these model melting regimes, which generate 5, 6, and 7 km of crust, respectively, bound essentially the entire field of observed East Pacific Rise (EPR) MORB compositions in SiO_2 and FeO* vs MgO. They also provide excellent fits to the bulk of the data in TiO_2, Al_2O_3, and CaO, although there is evidence in the natural data for these oxides of samples that experienced unusual (high-pressure?) fractionation histories involving early cpx fractionation [see also Grove *et al.* (1992)] and the liquid line of descent does not quite reproduce the average slope in the Al_2O_3–MgO diagram. There is considerably more

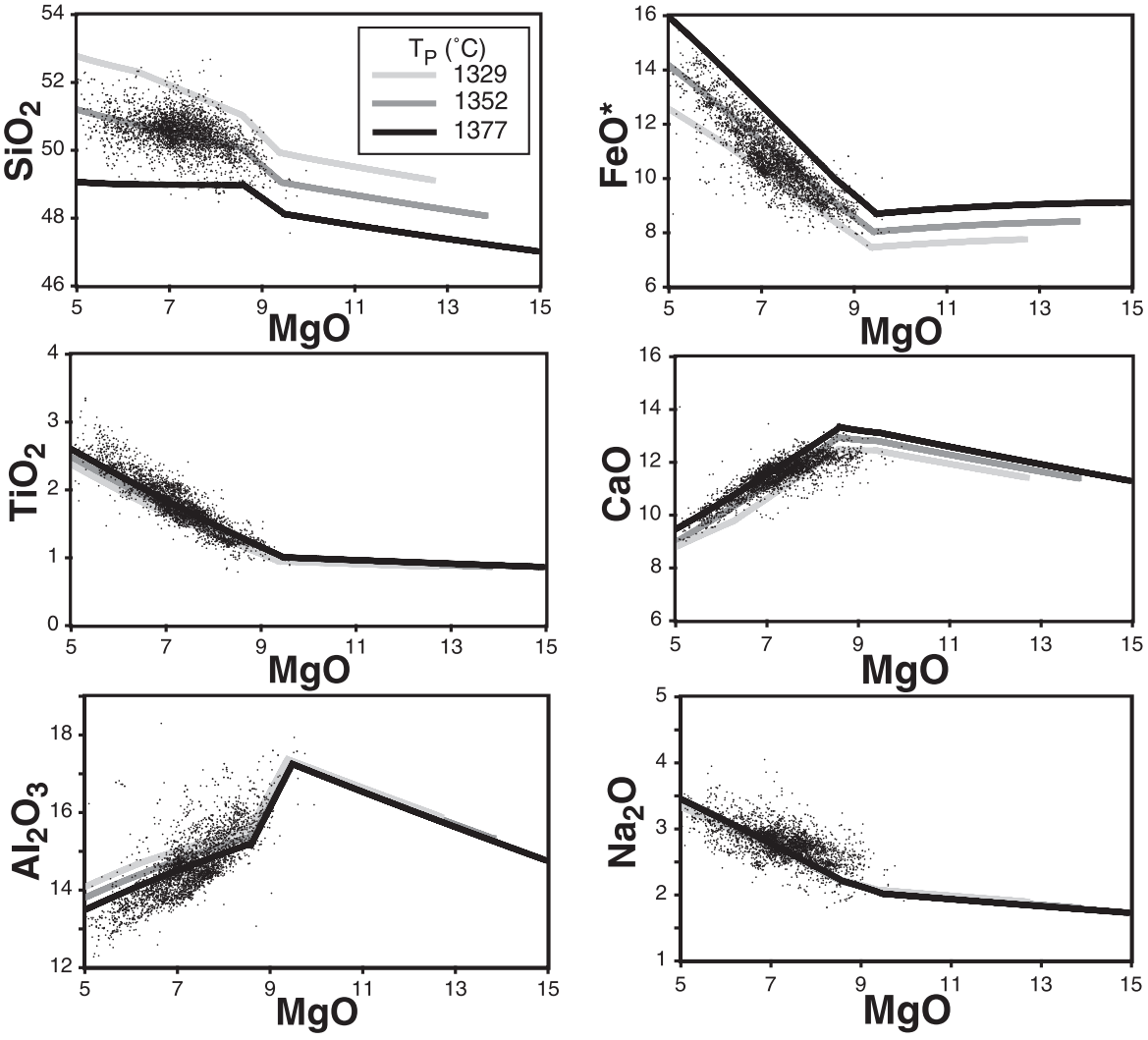

Fig. 1. Comparison of liquid lines of descent from primary aggregate liquids calculated by pMELTS with glass compositions from the East Pacific Rise (data and sources from petdb.ldeo.columbia.edu, Lehnert *et al.*, 2000); all axes are weight percent oxides. The source composition, crustal thicknesses, and primary aggregate liquid compositions for the three cases plotted are given in Table 2; the grey-scale shading of each liquid line of descent indicates the potential temperature of the melting regime from which it was generated. The method of calculating primary aggregate liquids and their fractionation path is given in the text.

variation in the Na_2O contents than can be explained with a constant depleted source composition in this model. At present, this model would require some source heterogeneity to generate the observed diversity along the EPR in Na_2O, as well as K_2O and P_2O_5. For the limited purposes of the present study, the point is that the primary aggregate liquids generated by polybaric fractional melting with pMELTS and tested for their liquidus relations are in fact reasonable parental MORB compositions.

The pMELTS model can also be used to simulate focused equilibrium porous flow, leading to formation of dunite channels as in the melt transport scenarios of Kelemen and coworkers. This reactive flow calculation was documented using MELTS by Asimow & Stolper (1999). The equilibrium porous flow calculations previously published simulate the merging of identical channels into larger channels, such that in effect all channels nucleate at the same depth and exhaust pyroxenes at the same depth. This study includes a new calculation to simulate a 'two-porosity' melting regime, by calculating polybaric fractional melting in the interchannel regions and adding the extracted fractional melts to the channels. This simulates a continuum of channel scales, each of which carries a different flux and exhausts pyroxene at a different pressure.

We require, in addition to the forward melting calculations, a method for the inverse calculation of liquidus phase relations. The most straightforward approach to

Table 2: pMELTS model primary aggregate liquids for comparison with EPR MORB

	1	2	3	(Source)*
T_P (°C):	1329	1352	1377	
Crustal thickness (km):	5·1	6·0	7·0	
SiO_2	49·22	48·14	47·05	46·16
TiO_2	0·85	0·85	0·85	0·171
Al_2O_3	15·91	15·34	14·73	3·95
Cr_2O_3	0·06	0·06	0·06	0·475
FeO*	7·74	8·39	9·09	7·56
MgO	12·75	13·86	15·07	38·21
CaO	11·41	11·38	11·25	3·19
Na_2O	1·89	1·79	1·71	0·233
H_2O†	(0·25)	(0·225)	(0·2)	—

*Source obtained from Hart & Zindler (1986) primitive upper mantle by extracting 1% melt.
†Water added to parental liquid to obtain appropriate fractionation path.

determining the equilibrium phase relations on a liquid isopleth (i.e. a constant bulk composition plane) would be simply to calculate isobaric, isothermal equilibria on a grid, and draw curves between distinct phase assemblages, much as an experimentalist does in interpreting a set of discrete experimental results. A more precise version of this calculation numerically follows each phase boundary with a subroutine that automatically searches at a sequence of pressures for the temperature at which a given phase appears. This leads to 'stable inverse phase diagrams', directly analogous to experimental results, some of which are shown below.

Stable inverse phase diagrams, however, may be difficult to interpret because of reaction relations among the phases. A liquid may be saturated with a phase on its liquidus at some pressure, but if that phase is an odd reactant (for example, olivine in the melting reaction cpx + opx + spinel = melt + olivine), it will not appear with falling temperature. Furthermore, a stable inverse phase diagram shows the progress of equilibrium crystallization of the liquid composition. During equilibrium crystallization, the evolution of liquid composition below the liquidus displaces the appearance of subsequently crystallizing phases in ways that obscure their proximity to saturation in the original liquid composition. This is demonstrated with two simple cases in Fig. 2. First, we consider the crystallization of liquid A in the system MgO–SiO_2 at low pressure (Fig. 2a). The liquid lies in the primary phase volume of forsterite, but from its liquidus temperature a relatively small undercooling would be required to saturate with enstatite, if forsterite crystallization were suppressed. On the equilibrium cooling path, however, the crystallization of forsterite shifts the liquid composition and delays the appearance of enstatite to the significantly lower peritectic temperature at point P. Thus a stable isopleth diagram would suggest that liquid A requires a large degree of undercooling to saturate with enstatite, whereas in fact it is the peritectic composition P (somewhat more SiO_2-rich than liquid A) that saturates with enstatite at this temperature. On the other hand, we consider liquid B in the same system at high pressure (Fig. 2b), where the liquid that coexists with forsterite and enstatite has moved past a singular point to more MgO-rich compositions and the forsterite–enstatite–liquid univariant becomes a eutectic at point E. Now liquid B is in the enstatite primary phase volume, is far from saturation with forsterite, and would require considerable undercooling to reach saturation in the absence of enstatite crystallization. On the equilibrium crystallization path, however, forsterite appears at the higher eutectic temperature. Here, the stable isopleth diagram showing the equilibrium crystallization path would suggest that liquid B is close to forsterite saturation, but actually shows instead where the eutectic liquid composition E is forsterite saturated. These examples show that, depending on the configuration of liquidus boundaries, crystallization of the liquidus phase can displace the appearance of the second phase to either higher or lower temperature relative to the saturation temperature of the latter phase in the original liquid.

To avoid these difficulties of interpretation, most of the pMELTS calculations in this paper show 'metastable inverse phase diagrams'. In other words, pMELTS can generate a set of saturation curves for each solid in the liquid of interest. This simply requires a search for the temperature where the affinity of each phase in the fixed liquid composition crosses zero, when crystallization of all other phases is suppressed. Although for all but the liquidus phase these curves are metastable, this type of diagram shows the true saturation state of the liquid, can be calculated rapidly, and avoids the complexities of reaction relations and crystallization paths that occur in determining stable inverse-method phase diagrams.

MAGPOX calculations

MAGPOX is basically a crystallization calculation with three important components. First is a series of parameterizations of liquidus boundaries in the pseudo-quaternary Olivine–Plagioclase–Wollastonite–Quartz system relevant to mafic or ultramafic compositions. The program tests the liquid composition against the liquidus boundary equations to determine which phases are saturated, and then calls the second component, a set of empirical partitioning algorithms, to calculate the

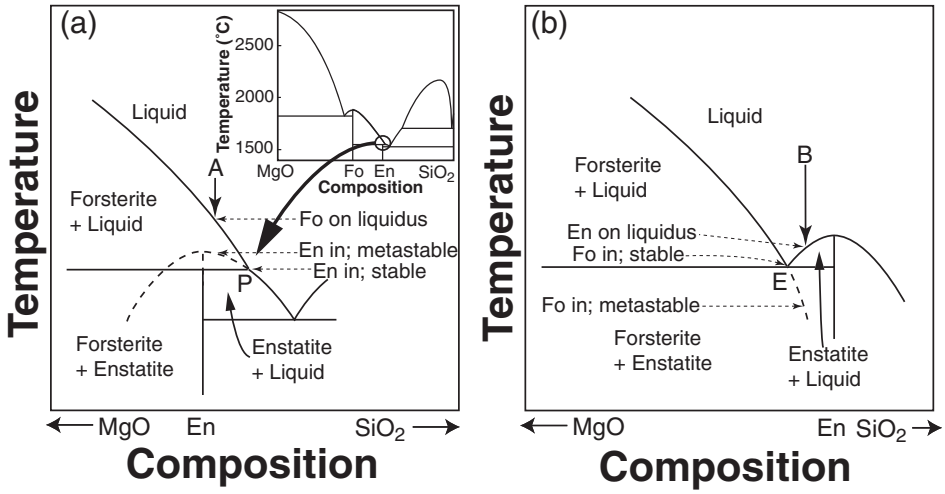

Fig. 2. A schematic illustration of the effects that crystallization of the liquidus phase can have on the temperature at which a second phase begins to crystallize, relative to the saturation temperature of the second phase in the original liquid composition. (a) The inset shows the temperature–composition phase diagram of the system MgO–SiO_2 at 1 atm pressure (Fo, forsterite; En, enstatite). The circled area is enlarged schematically to show relations around the peritectic point (P). In this case, liquid composition A has forsterite on the liquidus. If forsterite did not crystallize, enstatite would be saturated at the point shown on the metastable enstatite liquidus (dashed). However, because of forsterite crystallization, enstatite does not appear on the equilibrium cooling path until the peritectic temperature (P). Hence, in this case, the liquidus phase lowers the temperature of appearance of the second phase. (b) At higher pressure, the phase relations in this system change and create a eutectic where liquid E coexists with forsterite and enstatite; only a close-up of this area of the schematic phase diagram is shown. Liquid B has enstatite on the liquidus. On the equilibrium cooling path, forsterite appears at the eutectic temperature (E). However, if enstatite did not crystallize, then forsterite would not be saturated until the temperature indicated at the point on the metastable forsterite liquidus (dashed). Hence, in this case, the liquidus phase raises the temperature of appearance of the second phase. The metastable liquidus curves are therefore more reliable than the equilibrium isopleths as indicators of the saturation state of each phase in the original liquid composition.

major element composition(s) of the saturating phase(s). The third component is a set of empirical functions that vary the proportions of the saturating phases so as to maintain the liquid along the liquidus boundaries. Partial melting is simply the reverse of equilibrium crystallization. With minor changes in code the calculations were adapted to model a variety of igneous processes including simple fractional crystallization (Longhi, 1991), polybaric fractional fusion (Longhi, 1992), and fractional crystallization of a magma ocean (Longhi, 2003). The versions employed in this study are similar to BATCH described by Longhi (2002), but the phase boundary parameterizations have been revised to accommodate a new pressure calibration for piston-cylinder experiments with $BaCO_3$ pressure media (Longhi, 2004).

RESULTS

Batch melting

Let us begin with a trivial exercise, to show that the forward and inverse calculations from models of this type are in fact internally consistent and to prepare ourselves to interpret the more interesting cases to follow. We used pMELTS to calculate batch melting of the Hart & Zindler (1986) primitive upper-mantle peridotite composition at 1 GPa pressure and 1350°C temperature (compositions of sources and liquids used in the remainder of this paper are given in Table 3). The melt fraction of the resulting equilibrium is 13% and the liquid is a primitive basalt with 13·6% MgO. The Fe–Mg exchange K_D between olivine and liquid is found to be 0·333, which is similar to the value expected for a liquid with this MgO content (Herzberg & O'Hara, 2002). It should be noted that this calculation is somewhat too oxidizing for direct comparison with experimental melts of fertile peridotites at similar pressure, temperature and melt fraction in graphite or Fe capsules; at more reducing conditions pMELTS predicts a liquid with the SiO_2, Al_2O_3 and CaO concentrations in the liquid all $\sim$1 wt % (absolute) higher, and the FeO and MgO concentrations $\sim$1% lower.

Figure 3 shows the stable and metastable inverse phase diagrams for the liquid composition derived from this batch melting calculation. The diagrams show that the liquidus relations of this liquid recover the exact multiple saturation condition from which it was extracted, at the same pressure and temperature. Also, the mineral compositions on the liquidus at the multiple saturation point are identical to those in the residue of the forward calculation. Clearly, the system is well behaved: an exact multiple saturation point is necessary for this liquid to have been in equilibrium with this residue.

Comparison of Fig. 3a and b shows that the metastable inverse diagram is substantially easier to interpret.

Table 3: Compositions of mantle source and liquids studied by inverse method

	1	2	3	4	5	6	7	8	9
SiO_2	45·96	48·81	47·24	43·65	51·25	49·31	47·91	50·34	52·79
TiO_2	0·18	0·85	0·88	0·83	0·86	1·12	1·13	0·71	0·39
Al_2O_3	4·06	15·34	15·02	12·52	17·06	15·31	13·31	12·15	12·50
Cr_2O_3	0·47	0·08	0·08	0·08	0·08	0·28	0·33	0·34	0·22
FeO*	7·54	7·90	8·79	11·43	6·40	7·85	9·20	8·47	7·67
MgO	37·78	13·64	14·56	19·15	10·65	13·07	16·17	16·69	17·19
MnO	0·13	—	—	—	—	0·18	0·21	—	—
CaO	3·21	10·89	10·65	9·86	10·28	9·72	9·57	9·07	8·67
Na_2O	0·33	2·31	2·61	2·29	3·28	2·86	2·01	2·08	0·44
K_2O	0·03	—	—	—	—	0·47	0·38	—	—
Mg-no.		77·3	76·6	76·8	76·7	74·8	75·8	79·6	81·6
K_D		0·333	0·321	0·303	0·349	0·326	0·333	0·348	0·386
Crustal thickness (km):		—	7·0	11·4	3·8	5·3	9·9		
Mean extent of melting F_B:		0·13†	0·090	0·094	0·070	0·115	0·122		
Mean pressure of melting (GPa):		1·0†	1·17	1·79	0·75	1·3	1·8		
Forsterite content of liquidus olivines:		91·1	91·2	91·6	90·9	90·1	90·4	91·8	92·0
Forsterite content of olivine in most advanced residue:		91·1	91·8	92·4	91·4	91·3	91·5	91·8	92·0

1, Peridotite source composition, from Hart & Zindler (1986). 2, Batch melt of composition 1 at 1 GPa, 1350°C, from pMELTS. 3, Polybaric aggregate fractional melt from pMELTS, $P_o = 2{\cdot}16$ GPa ($T_P = 1367$°C). 4, Polybaric aggregate fractional melt from pMELTS, $P_o = 3{\cdot}5$ GPa ($T_P = 1443$°C). 5, Polybaric aggregate fractional melt from pMELTS, $P_o = 1{\cdot}5$ GPa ($T_P = 1282$°C). 6, Polybaric aggregate near-fractional melting from MAGPOX, $P_o = 2$ GPa. 7, Polybaric aggregate near-fractional melting from MAGPOX, $P_o = 3$ GPa. 8, 50× focused equilibrium porous flow channel melt from pMELTS ($T_P = 1443$°C). 9, 50× focused fractional porous flow channel melt from pMELTS ($T_P = 1443$°C). Mg-number = molar 100 × MgO/(MgO + FeO). K_D = molar $(MgO/FeO)^{olivine}/(MgO/FeO)^{liquid}$.
†Actual, not mean, extent and pressure of melting for batch melt composition 2.

Figure 3a is a stable phase diagram showing actual equilibrium crystallization assemblages at each pressure and temperature. Reading of this diagram is complicated by the pinching-out of the olivine phase field at the multiple saturation point. At 1 GPa, olivine is in a reaction relationship analogous to the peritectic point in Fig. 2a, and it does not crystallize with falling temperature. The metastable inverse diagram in Fig. 3b shows the saturation curve of each phase in the liquid composition, independent of the others. This results in a smooth olivine saturation curve that crosses through the multiple saturation point without a kink. In the stable phase diagram, Fig. 3a, spinel crystallizes as the second phase in the olivine liquidus field. Energetically, however, spinel is further from saturation in this liquid than either pyroxene, as seen in the low-pressure part of the metastable inverse diagram, Fig. 3b, where spinel saturation requires more undercooling than opx or cpx. Furthermore, in the stable inverse diagram (Fig. 3a), opx crystallization is suppressed to lower temperature relative to its saturation point on the metastable diagram (Fig. 3b), by either olivine or cpx crystallization, similar to the effect seen schematically in Fig. 2a. For simplicity in locating close approaches to multiple saturation, pMELTS calculations below are presented only as metastable inverse phase diagrams.

Polybaric fractional melting

pMELTS

In the next exercise, the same fertile source peridotite as in the previous example is decompressed isentropically from high pressure until it encounters its solidus. Thereafter, as in the calculations of candidate MORB parents in Fig. 1, incrementally adiabatic polybaric fractional melting and passive-flow integration are used to obtain an aggregate primary liquid composition. Let us emphasize that this aggregate liquid composition was never in equilibrium with a mantle residue at any condition, although it is a mixture of liquids that were each in equilibrium with lherzolite or harzburgite at the various conditions from which they were drawn.

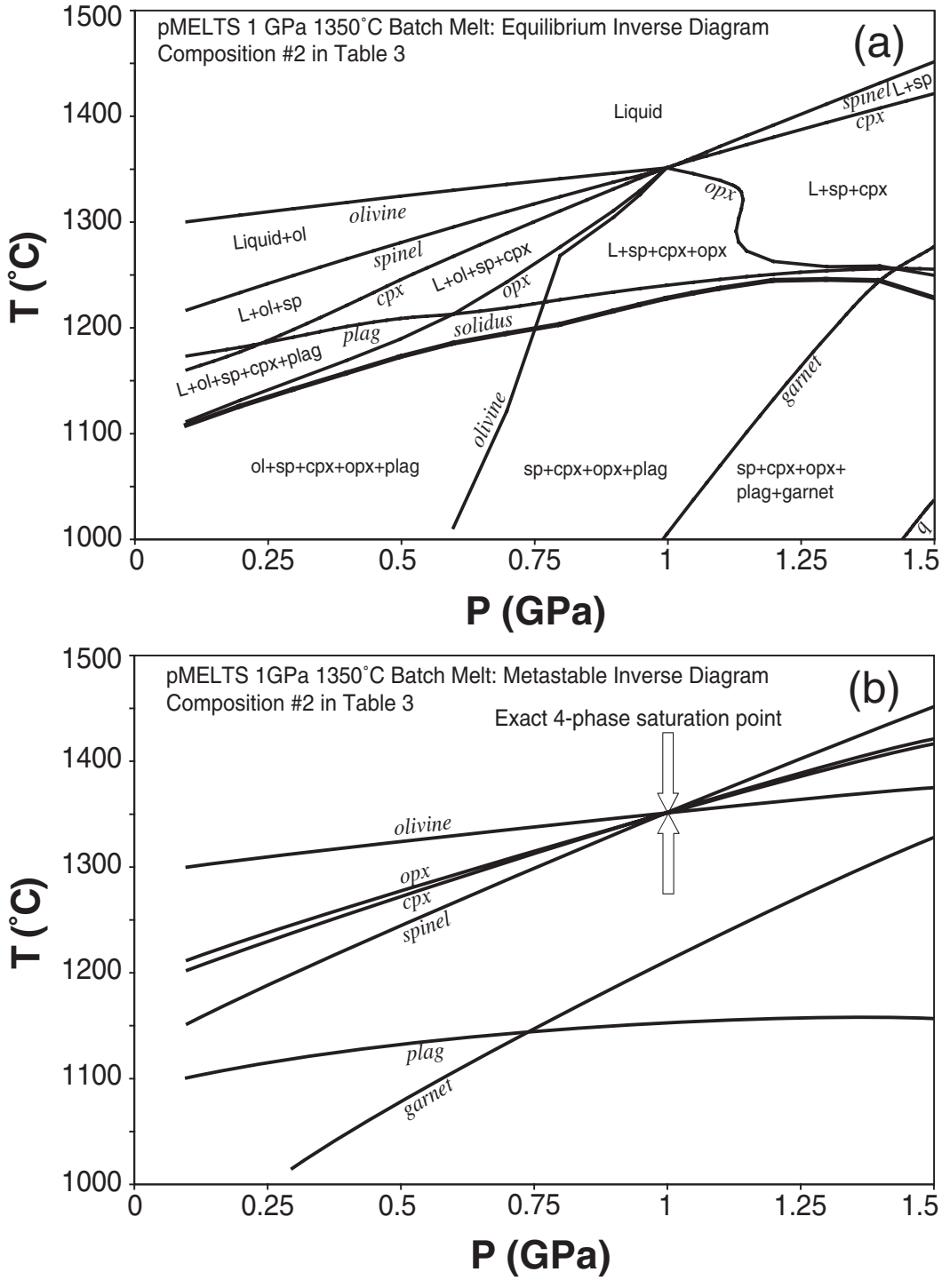

Fig. 3. Inverse phase diagrams for the liquid (composition 2 in Table 3) obtained from batch melting of source peridotite (composition 1 in Table 3) at 1 GPa, 1350°C according to pMELTS. The extent of partial melting is 13% by mass. (a) Stable phase relations. The curves labelled with phase names in italics show the upper temperature limit of each phase, except for the solidus curve indicating the lower limit for liquid and the lower limb of the olivine curve indicating complete resorption of this phase. These curves bound fields of distinct phase assemblages, as labelled. It should be noted that the olivine (ol), orthopyroxene (opx), clinopyroxene (cpx), and spinel (sp) curves all meet at 1 GPa, 1350°C, even though olivine does not form on cooling at this temperature and this is the only point where opx-in touches the liquidus. (b) Metastable phase relations. These curves show the temperature at which each phase is saturated in the bulk liquid composition, ignoring the potential crystallization of any other phases. Again, the olivine, opx, cpx, and sp curves cross precisely at 1 GPa, 1350°C; the multiple saturation point is highlighted by the white block arrows. The diagrams also show stability or saturation curves for plagioclase feldspar (plag), garnet, and quartz (q).

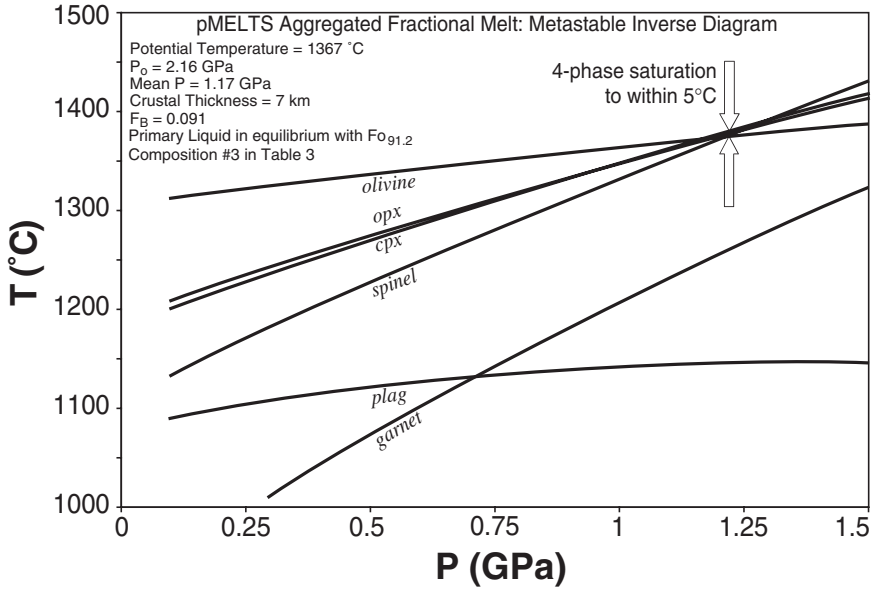

Fig. 4. Metastable inverse phase diagram for the liquid (composition 3 in Table 3) generated by polybaric fractional melting of the source peridotite at the same potential temperature as the batch melting equilibrium shown in Fig. 2, according to pMELTS. Melting begins at 2·16 GPa and continues to the base of the resulting crust at 7·0 km or 0·18 GPa. The residual assemblage is spinel lherzolite until 0·6 GPa, where cpx is exhausted. About 6% of the total melt that contributes to the aggregate comes from harzburgite melting. The four saturation curves for olivine, cpx, opx, and spinel come within 5°C of each other at the point highlighted by the white block arrows.

Standard MORB case. At a potential temperature (McKenzie & Bickle, 1988) $T_P = 1367°C$, the fertile source composition encounters its solidus at 2·16 GPa and melting is continued to the base of the crust. This melting path, in a passive-flow ridge geometry, generates a 7 km thick igneous crust and the mean extent of melting is 0·09. The mean pressure from which the increments of liquid were drawn to make the aggregate liquid is 1·17 GPa. This aggregate liquid composition (Table 3, composition 3) yields the metastable inverse phase diagram shown in Fig. 4. Remarkably, the liquidus curves for the four phases olivine, opx, cpx, and spinel approach to within 5°C of one another at 1·2 GPa. Considering only olivine–opx–cpx co-saturation, which might frequently be interpreted in experimental data as sufficient to show lherzolite multiple saturation, these three curves approach to within 1°C at 1·15 GPa. The 5°C difference in saturation temperatures between the four phases in this model is finer than the resolution of any plausible experimental effort to determine the phase relations of a given liquid composition. The model therefore shows that a blindly selected and heuristically reasonable process (not, we emphasize, an intentional construction) that did not involve equilibration of a liquid with a mantle assemblage can nevertheless yield a liquid that satisfies the necessary conditions for such equilibration to better than experimental precision. Remarkably, the near multiple saturation pressure found, 1·15–1·2 GPa, is in excellent agreement with the actual mass-weighted mean pressure of melt extraction, 1·17 GPa. Therefore, this test shows that the inverse method works well in this case as a means of discovering the average conditions of equilibration. It also shows, however, that there is a danger of over-interpreting an experimental multiple saturation result as proof that an aggregate primary liquid is in fact a single mantle-equilibrated primary liquid.

Sensitivity to fractional crystallization. One complexity that arises in using measured natural glass compositions to infer the conditions of magma genesis is the correction for low-pressure fractionation. These problems are minimized if the glass is primitive enough to have fractionated only olivine, as back-addition of liquidus olivine is a well-constrained procedure (e.g. Albarède, 1992). Back-addition of liquidus olivine is continued incrementally with rising temperature, and increasing MgO content and olivine Mg-number, until equilibrium with a proposed mantle residue is reached; the resulting liquid is then parental to the observed suite and also plausibly primary. However, the exact forsterite content (i.e. Mg-number) of the residual olivine is not known. In fact, for a fractional melting model, there is no single residual olivine composition. Nevertheless, observations of abyssal peridotites suggest that a range of 90–91·6 is appropriate. In the above exercise, we used the primary aggregate liquid (in equilibrium with $Fo_{91·2}$ olivine on its 1 bar liquidus; see Table 3), without any forward- or back-fractionation. In fact, this liquid is an aggregate of

increments of liquid that were extracted from residues ranging from $Fo_{90·3}$ at the solidus to $Fo_{91·8}$ in the most advanced residue at the base of the crust. To investigate the effects of slight differences in the fractionation correction of a measured composition, such as one might make in testing the hypothesis that the parent of a given liquid is multiply saturated, we also looked at the metastable inverse phase relations of the liquids obtained by forward- or back-fractionating the primary aggregate liquid to equilibrium with olivines in the range Fo_{90} to Fo_{92}. The existence of an apparent multiple saturation point is relatively insensitive to the exact fractionation correction in this range. The 5°C range at closest approach to four-phase multiple saturation decreases to a minimum of 3·5°C for the liquid cooled 7°C below the 1 bar liquidus to equilibrium with $Fo_{91·0}$ olivine (about 1·5% crystallization). However, the location of the closest approach to multiple saturation is strongly sensitive to errors in fractionation correction, and shifts to lower pressure with decreasing Mg-number of the estimated primary melt, by about 0·1 GPa for every 0·1% change in the forsterite content of the liquidus olivine. We conclude that, when mean pressure of melting is inferred from multiple saturation of an aggregate liquid, the inferred pressure may be substantially in error if there has been any modification of the melt by olivine crystallization or if the correction for such crystallization is performed approximately.

Sensitivity to potential temperature. To test whether the close approach to multiple saturation seen in the pMELTS polybaric fractional result above is limited to a narrow range of potential temperature, we repeated the calculation twice: for a hotter mantle that intersects its solidus at 3·5 GPa ($T_P = 1443$°C; composition 4 in Table 3) and for a colder mantle that intersects its solidus at 1·5 GPa ($T_P = 1282$°C; composition 5 in Table 3). The metastable liquidus phase relations of these aggregate liquid compositions are shown in Fig. 5. In the hotter case (Fig. 5a), as might be expected for a liquid that is a mixture of melt increments in equilibrium with garnet-bearing and garnet-free residues, the spinel surface is displaced to somewhat lower temperatures and the garnet surface to higher temperatures. The closest mutual approach of the four phase boundaries ol, opx, cpx and sp is within 15°C at 1·9 GPa. This could perhaps be distinguished experimentally from multiple saturation, although larger temperature intervals have been interpreted otherwise (e.g. Green *et al.*, 1979). On the other hand, the three-phase assemblage ol–opx–cpx still shows a common saturation point to within 1·5°C at 1·7 GPa and the literature shows that experimental observation of such a three-phase point might be interpreted as demonstrating conditions of equilibration with a mantle residue (e.g. Bender *et al.*, 1978). The actual mean pressure of extraction in this hot case is 1·79 GPa, so again the liquidus relations of the aggregate liquid do faithfully record the mean pressure of derivation. In the colder case (Fig. 5b), the olivine saturation curve shifts downwards whereas the spinel and plagioclase curves shift upwards. The result is a close approach to four-phase multiple saturation at 0·7 GPa, which is again similar to the mean pressure of extraction, 0·74 GPa.

We conclude, at least within the self-consistent context of pMELTS, and at least where the primary aggregate liquid is known exactly with no fractionation or post-melting modification other than mixing, that mixtures often cannot be distinguished from mantle-equilibrated liquids using their liquidus relations, but that near-multiple saturation points, when they do occur, faithfully record the approximate mean pressure of melt extraction.

MAGPOX

We performed similar polybaric near-fractional melting calculations using MAGPOX. The Hart & Zindler (1986) primitive upper-mantle composition was decompressed from solidus intersections at 2 GPa and 3 GPa, respectively. The calculations proceeded in 0·05 GPa steps to a final melting pressure of 0·6 GPa and the amount of melting in each step was approximated by balancing the fall in melt temperature relative to a 15·0 K/GPa adiabat against the temperature equivalent of the heat of fusion as suggested by Hess (1992). All of the melt generated above a residual porosity fraction of 0·002 was subtracted from the depleting source and added to the pooled melt reservoir. Typically, the amount of melt extracted in each step was 25–70% of the melt generated. At the end of each fractional fusion calculation we summed the pooled melts according to the two-dimensional triangular geometry of Plank & Langmuir (1992), and then calculated the equilibrium phase relations for each triangular liquid (Table 3, compositions 6 and 7) at 0·05 GPa intervals from 0·5 to 3·0 GPa (Fig. 6a and b).

In its current configuration MAGPOX is designed only for compositions with olivine on their liquidus. Peridotites are thus appropriate, as are most primitive basalts at low to intermediate pressure. For the present purposes, we present the calculated phase relations of the two aggregate melts directly for pressures up to the point where olivine disappears from the liquidus surface. We extrapolated the various sub-liquidus curves calculated at lower pressures into the higher-pressure zone, modifying the curves as necessary to produce a thermodynamically correct topology of liquidus equilibria. The calculated diagrams are thus equivalent to those that would be generated by melting experiments.

In both cases olivine is the liquidus phase at low pressure and is replaced in succession along the liquidus by orthopyroxene and clinopyroxene. In the 2 GPa case, the aggregate primary liquid shows liquidus boundaries for

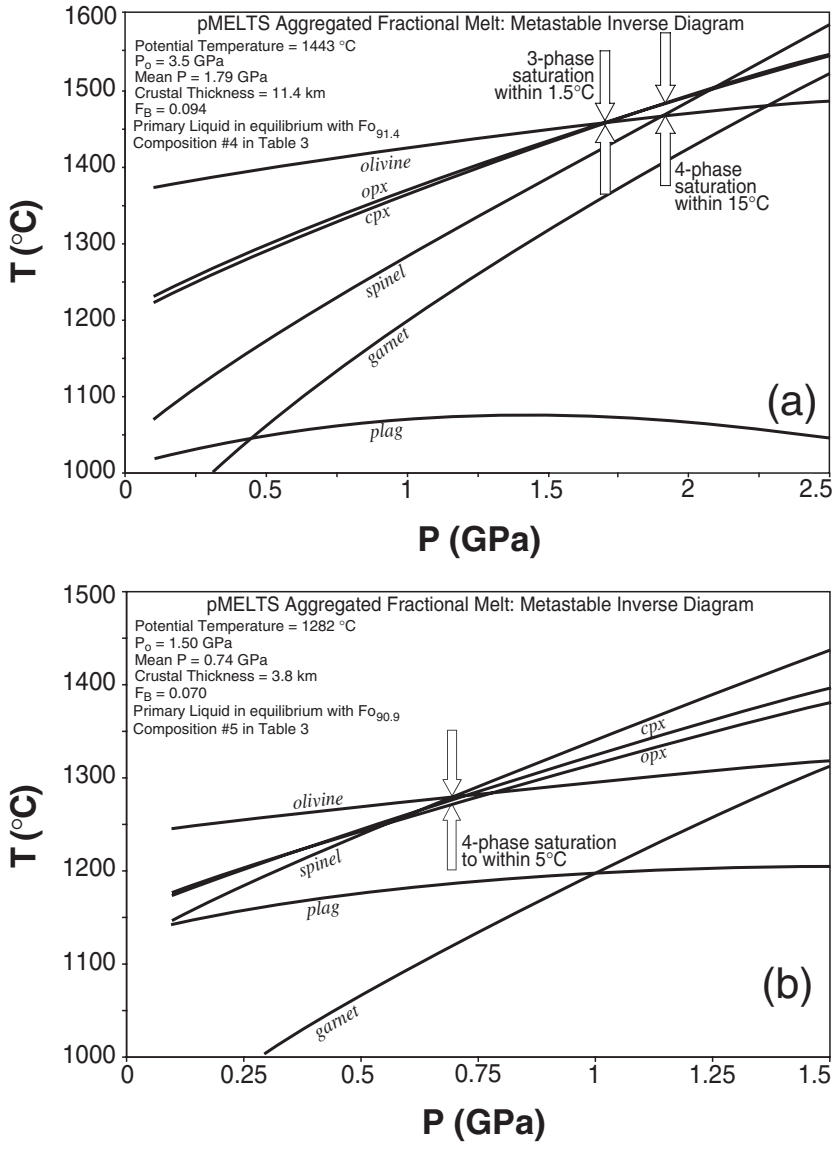

Fig. 5. (a) Metastable inverse phase diagram for the liquid (composition 4 in Table 3) generated by polybaric fractional melting of the source peridotite at a higher potential temperature than the case in Fig. 3, according to pMELTS. Melting begins at 3·5 GPa and continues to the base of the resulting crust at 11·4 km or 0·29 GPa. The residual assemblages are garnet + spinel lherzolite until 3·1 GPa (4% of the melt), spinel lherzolite until 1·0 GPa (86% of the melt), and spinel harzburgite thereafter (10% of the melt). The closest approaches to three-phase (olivine + opx + cpx) and four-phase (olivine + opx + cpx + sp) saturation are highlighted. (b) Metastable inverse phase diagram for the liquid (composition 5 in Table 3) generated by polybaric fractional melting of the source peridotite at a lower potential temperature than the case in Fig. 3, according to pMELTS. Melting begins at 1·5 GPa and continues to the base of the resulting crust at 3·8 km or 0·10 GPa. The residual assemblages are spinel lherzolite (57% of the melt), plagioclase lherzolite (27%), and spinel harzburgite (16%). The closest approach to four-phase (olivine + opx + cpx + spinel) saturation is highlighted.

ol, opx, and cpx that approach each other within 10°C at 1·8 GPa, and spinel joins the other three within 20° of the liquidus. In the 3 GPa case, the aggregate primary liquid has the four phases ol, opx, cpx, and garnet within 10°C of the liquidus from 2·5 to 2·7 GPa. In fact, this composition approaches within 15°C of five-phase saturation with ol, opx, cpx, gt, and sp at 2·5 GPa. These calculations are included here to show that the appearance of near-multiple saturation points in polybaric aggregate liquids is not merely an artefact of pMELTS; it also arises in the independent description of liquidus boundaries parameterized in MAGPOX. We also verified that this kind of multiple saturation point is not some kind of unforeseen yet inevitable consequence of the construction of MAGPOX by examining the liquidus relations of the aggregate fractional melt of a lunar source mantle

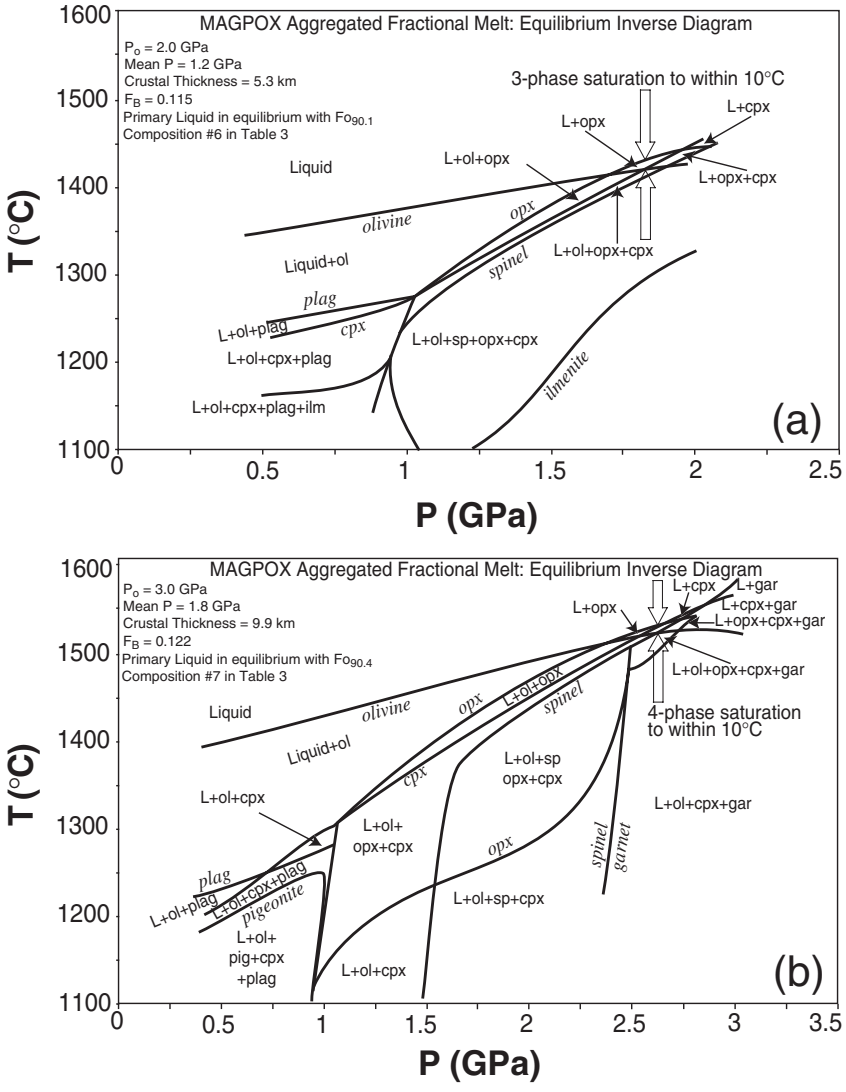

Fig. 6. Stable inverse phase diagrams for aggregate primary liquids from triangular polybaric fractional melting regimes according to MAGPOX. (a) Melting of the source composition begins at 2·0 GPa, yielding aggregate liquid composition 6 in Table 3. (b) Melting begins at 3·0 GPa, yielding aggregate liquid composition 7 in Table 3. Melting in both calculations terminates at 0·6 GPa. ilm, ilmenite; gar, garnet; pig, pigeonite.

proposed by Longhi (1992) as the parent of the lunar green glass. The olivine and orthopyroxene saturation curves of this composition cross at 2·0 GPa, but cpx is everywhere at least 150°C below the liquidus. Plagioclase and garnet saturation occur another 50–100°C lower still. We conclude that the near approach to multiple saturation obtained for aggregate fractional melts of the terrestrial mantle is not inevitable; we discuss below whether it is mere coincidence or something more.

Channelized porous flow

Although a near-fractional melting process is generally considered to be closer to reality than any single-primary-liquid paradigm, the specific model of perfect fractional melt transport is itself physically questionable. Even though liquids may begin to migrate by porous flow at low melt fraction (McKenzie, 1985*b*), they should continue to interact chemically with the solids (Spiegelman & Kenyon, 1992). A reasonable hypothesis that incorporates this reasoning and also explains the gross disequilibrium between primitive MORB and opx at low pressure is that most of the liquid reaching the oceanic crust has migrated through high-flux channels free of pyroxenes and hence only equilibrated with olivine and spinel beyond a certain point (Kelemen *et al.*, 1997). In such a scenario the coincidence of a primitive MORB with a multiply saturated liquid in projection from olivine might be taken to identify the location where melt was channelized, or where the channels carrying the melt exhausted

orthopyroxene. In other words, once a melt begins migrating through a channel containing only olivine and spinel, the only degrees of freedom available to change its composition are in the plane defined by the initial melt, olivine, and spinel. Assuming crystallization or assimilation of spinel is limited to a few percent, projection from olivine should then be able to co-locate the final melt composition emerging from the top of the channel with the melt composition in the channel at the depth where opx was last encountered. The metastable inverse phase diagram may provide a kind of energy–space projection, in that it shows where opx is saturated in the liquid independent of the energetic effects of olivine–spinel crystallization, much as projection from olivine and spinel would normalize the compositional effects of addition or removal of these phases. When applied to an actual primitive measured liquid, this would produce a meaningful result only in the case where either a single channel carried the sampled liquid or all the channels that contributed melt were identical (in that they exhausted opx at the same depth).

We tested this idea using the focused equilibrium porous flow simulations of channelized flow developed by Asimow & Stolper (1999). This model performs a sequence of batch melting equilibria at regular increments in pressure, with the mass (or flux) of liquid multiplied by a small factor and the reference entropy adjusted to account for the added melt at each step. The focused melt column is characterized by an overall focusing factor; thus if there are 350 steps between the solidus at 3·5 GPa and the surface, a focusing factor of 50 implies that the melt mass is multiplied by the 350th root of 50 at each step. For this example, the hot mantle case (T_P = 1443°C) was adopted and the focusing factor was set to 50. The fractional melting calculation at the same potential temperature exhausted cpx at 0·97 GPa and retained a harzburgite residue at the base of the crust. In the high-flux channel simulation, however, cpx is exhausted at 1·37 GPa and opx at 0·96 GPa. The metastable inverse phase relations of the final composition to emerge from this channel (composition 8 in Table 3) are plotted in Fig. 7a. By construction, this liquid is co-saturated with olivine and spinel at 0·2 GPa where it was extracted from the dunite channel. Furthermore, as expected, the liquid drawn from a dunite channel that last contained opx at 0·96 GPa shows an intersection of the olivine and opx saturation curves at a similar pressure, 1·05 GPa. This suggests that the metastable inverse diagram indeed acts approximately like a projection from olivine. It also implies that the pressure of opx exhaustion in a channel system can perhaps be approximately inferred from the liquidus relations of the primitive liquid exiting the channel (but see the two-porosity case below).

However, the cpx saturation curve is surprisingly close to the olivine + opx point, only 8°C below, despite the 0·4 GPa gap between the exhaustion of the two pyroxenes in the forward calculation. It is puzzling that the liquid did not evolve further from cpx saturation once cpx was exhausted from the channel residue, and shows again that close proximity of saturation curves can arise without actual equilibration having occurred with the phases in question.

Two-porosity flow

The simulation of channelized porous flow performed by Asimow & Stolper (1999), and repeated above, multiplies the flux of batch melt through the system without changing its composition at the point of focusing. This simulates a channel network in which all channels nucleate at a common depth, each channel remains identical to adjacent channels at each depth, and large conduits grow by merging of such identical neighbouring conduits. However, observations of U-series disequilibria in MORB (see Lundstrom, 2000) and of abyssal peridotites (see Asimow, 1999) seem to require a so-called two-porosity system in which either a spectrum of channels nucleate at different depths or near-fractional melts are contributed to the channels at all depths. In this case the aggregate liquid exiting the channel system need not have last seen pyroxene at any particular pressure. That is, even though the high-flux conduit may have exhausted pyroxenes and become a dunite at, say, 1 GPa, a significant fraction of the melt emerging from the top of the channel was withdrawn at lower pressure from the lherzolite or harzburgite surrounding the channel and undergoing near-fractional melting.

We simulated this situation by modifying the focused flow calculation so that the liquid added to the channel at each depth is the product of fractional melting of the interchannel peridotite, rather than the liquid carried by an adjacent equilibrium flow channel. The calculation was performed at the same potential temperature and focusing factor as the previous model, the only change being whether equilibrium or fractional melt is added at each focusing step. In this channel, cpx is exhausted at 1·32 GPa and opx at 0·90 GPa. The metastable inverse phase relations of the final liquid to emerge from the channel are shown in Fig. 7b.

The phase relations of the aggregate liquid emerging from the fractional melting channel are similar to those of the liquid produced by the equilibrium-focusing channel. Both are, by construction, co-saturated with olivine and spinel at 0·2 GPa. Both have an olivine–opx intersection, although in the fractional case this occurs at lower pressure, 0·73 GPa. Both require only a few degrees undercooling below the ol–opx point to add cpx saturation. Both are very far from garnet or feldspar saturation (feldspar is off-scale below 1000°C in Fig. 7b). The lower pressure of the ol–opx point in

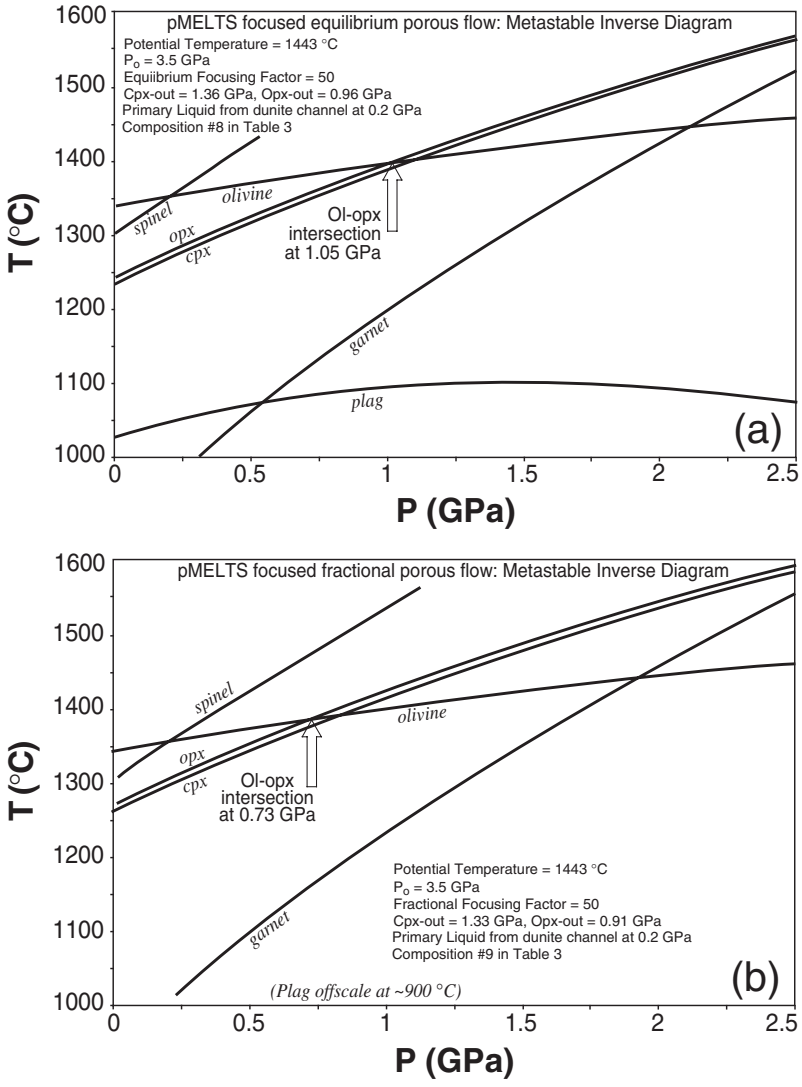

Fig. 7. Metastable inverse phase diagrams for the aggregate liquids produced by (a) a focused equilibrium porous flow calculation based on merging of identical channels (composition 8 in Table 3) and (b) a focused porous flow calculation drawing on fractional melts from the interchannel regions (composition 9 in Table 3). Both liquids are co-saturated with olivine and spinel at 0·2 GPa by construction. The pressure where the olivine and opx saturation curves intersect resembles the pressure of opx saturation that would be inferred by examination of a projection from olivine.

Fig. 7b compared with Fig. 7a is consistent with the significant contribution to the fractional channel calculation of liquid increments extracted from opx-bearing residues at low pressure. In some sense, this intersection pressure represents a kind of average over the liquid increments contributed to the channel of the last pressure at which each increment equilibrated with opx. However, this calculation shows that one cannot necessarily tell from the liquidus phase relations of the channel liquid whether it was extracted from a single-channel system like that in Fig. 7a or from a two-porosity system like that in Fig. 7b. That is, the olivine–orthopyroxene saturation curves intersect whether or not the liquid was in fact in equilibrium with both these phases at any specific pressure.

DISCUSSION

These exercises show that, insofar as pMELTS and MAGPOX provide internally consistent representations of phase relations, near-multiple saturation points can occur in mixed liquids even though these were never equilibrated with residual phases. In other words, the observation of multiple saturation (within experimental resolution) on the liquidus of a primitive liquid is not sufficient to prove that the liquid equilibrated with a

mantle assemblage without subsequent mixing. This is the answer to the question posed at the beginning of this paper. It remains to consider how this result arises. It could be just a matter of luck that the integrated liquids from polybaric fractional melting paths happen to lie near multiple saturation surfaces, perhaps for no systematic reason. Another possibility is that the multiple saturation surface has very little curvature, so that mixtures drawn from the surface are still near the surface. This result would arise by construction in a linear parameterization of saturation surfaces (e.g. Kinzler & Grove, 1992; Kinzler, 1997) where the locus of multiply saturated compositions is a hyperplane in composition space, with no curvature. Both MAGPOX and pMELTS have nonlinear parameterizations of liquidus surfaces, so such linear mixing does not arise in these models by construction, although it might still be approximated in practice. Whether something like this explains the pMELTS result is difficult to evaluate because the spinel peridotite saturation surface in the natural, high-variance system depends on composition, evolves during fractional melting, and does not, according to pMELTS, project to a well-defined cotectic. However, Duhem's theorem requires that the locus of liquids that arise by batch melting of a fixed bulk composition must define a surface in composition space, so let us try to examine this surface in a suitable projection space, in order to evaluate its curvature and to compare the fractional melting paths and integrated fractional melts with the surface in composition, rather than energy (as in Figs 3–7) space.

Figure 8 shows two projections of the CIPW normative tetrahedron olivine–diopside–plagioclase–silica (Walker *et al.*, 1979). The surface of liquids generated by batch melting of the peridotite source (composition 1 in Table 3) according to pMELTS is defined by the array of isobaric and equal melt-fraction contours. The isobars are labelled by pressures in GPa; the equal-melt fraction contours are colour-coded and labelled by mass extent of melting, *F*. The major features of this surface are: all the isobars end at the bulk composition of the source peridotite, a point near the olivine apex; olivine is the liquidus mineral up to 2·3 GPa so the isobars below this pressure collapse onto a line radial from the olivine apex at high melt fraction; all the isobars with solidi in the spinel or garnet lherzolite fields begin at very silica-deficient compositions off scale to the right in projection from diopside; in projection from silica it is clear that the cpx-out contour near 20% melting forms a cusp bounding the spinel lherzolite and spinel harzburgite saturation surfaces; liquids coexisting with plagioclase lherzolite are nearly univariant and form a well-defined cotectic curve bounding the low-pressure edge of the surface. The filled black circle shows the pMELTS batch melt at 1 GPa and 13% melting (composition 2 in Table 3; see Fig. 3), which naturally sits on the surface along the 1 GPa isobar and between the $F = 0{\cdot}10$ and $0{\cdot}15$ contours.

The loci of liquids generated along the pMELTS polybaric fractional melting paths are shown in Fig. 8, as are the two-dimensional aggregate liquids obtained by summing along these paths (i.e. compositions 3–5 in Table 3; see Figs 4 and 5). In both projections, the aggregate liquid points plot near the isobar where the multiple saturation points were observed in their metastable inverse phase diagrams, which is consistent with these liquids lying near the saturation surface for the original bulk composition. The curvature of the spinel lherzolite surface is hard to see in projection from diopside; however, it is evident in projection from silica that this surface is not a plane, and that there is no systematic reason for mixtures of liquids drawn from the surface also to lie on the surface. Furthermore, the projection from silica shows that the locus of fractional liquid increments departs from the batch melting surface, both before cpx-out and, most dramatically, after cpx-out. The paths of fractional increments are curved, and the aggregate liquid lies at least somewhat off the path in each case. However, it appears that the admixture of a series of liquids near the outside of the convex spinel lherzolite surface with a few percent of liquids (from harzburgite melting) far to the convex side are able to yield points that happen to lie close to the surface. We interpret these projections as evidence that our result, that mixtures of polybaric fractional liquids can mimic the saturation state of batch melts, is a logical consequence of the shape of the batch saturation surface and the weighted averaging involved in the polybaric calculation, but is by no means a construction or a tautology. An element of bad luck is involved; it seems perhaps that nature has conspired against us to allow for liquidus relations that are subject to over-interpretation.

CONCLUSIONS

(1) In perfectly fractional polybaric melting models generated with two independent descriptions of phase equilibria, multiple saturation with three or four phases can occur to good approximation in mixed liquids even though these mixtures were never equilibrated with solid phases. This result is not required by any underlying constraints, but arises from the particular shapes of the saturation surfaces and fractional liquid trajectories for peridotite melting. That two independent models, pMELTS and MAGPOX, with very different methods of describing saturation surfaces both yield apparently coincidental near-intersections indicates that experimental multiple saturation in a primitive liquid is not sufficient to demonstrate that it equilibrated with a mantle residue without subsequent modification.

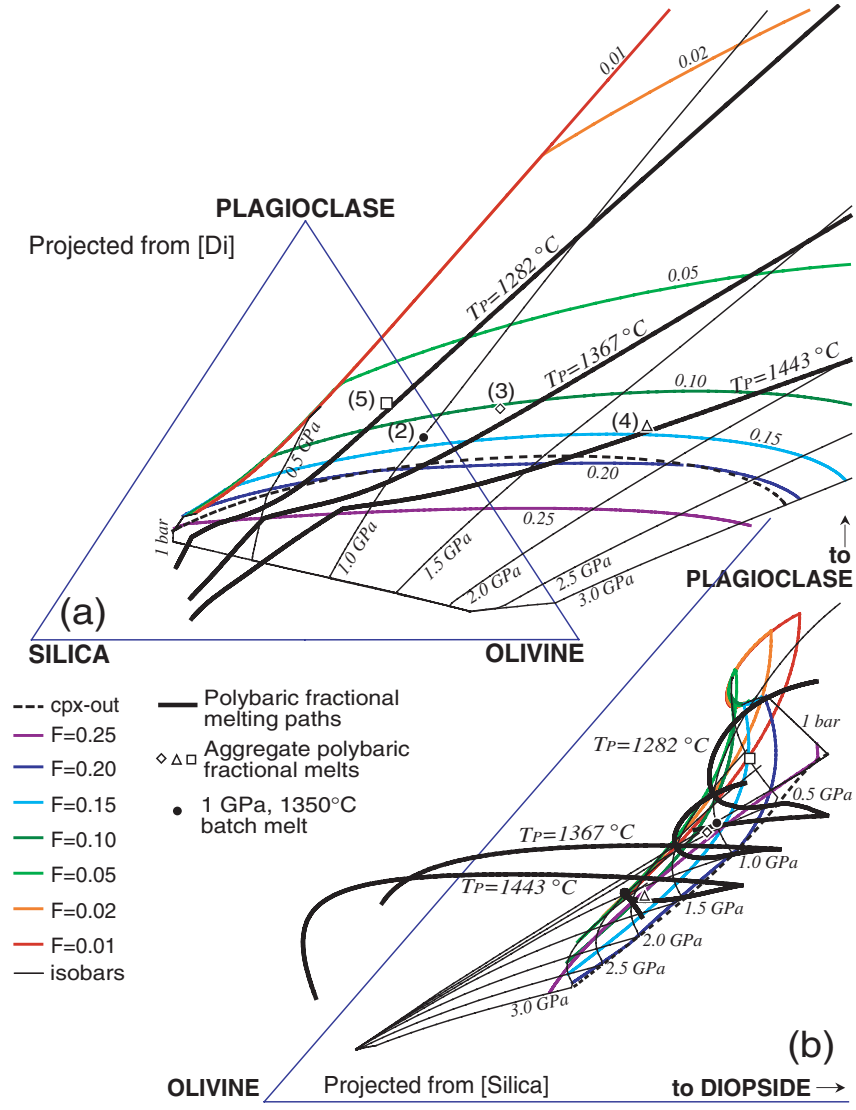

Fig. 8. Projections of the CIPW normative tetrahedron olivine–diopside–plagioclase–silica from (a) the diopside apex and (b) the silica apex, using the method of Walker *et al.* (1979). The surface of liquids generated by batch melting of fertile peridotite (composition 1 in Table 3) according to pMELTS is outlined by two sets of intersecting contours: the fine black lines are isobaric melting paths from solidus to liquidus, labelled by pressure, whereas the heavy coloured contours connect points of equal extent of melting by mass (F). •, Batch melt at 1 GPa and 1350°C, at $F =$ 0·13. The bold dashed black line marks the exhaustion of cpx from the residue, and bounds the lherzolite and harzburgite saturation surfaces. The three bold black curves show the sequence of incremental liquids and the open symbols show the passive-flow aggregate primary melt generated by polybaric fractional melting according to pMELTS at $T_P = 1282$°C (□), 1367°C (◇) and 1443°C (△), respectively. This figure is intended to help visualize the inference that the multiple saturation surface is not planar and hence there is no strict geometric construction that causes the aggregate fractional liquids to plot near the batch melting surface.

(2) The inverse method of experimental petrology, as a tool to directly identify the unique condition of origin of a basaltic liquid, is therefore subject to over-interpretation. Although the liquidus relations of primitive basalts do preserve information about the average conditions from which their constituent liquid increments were extracted, this may in fact be only an average condition and not a unique extraction point, even when multiple saturation is found.

(3) In the contemporary generation of channelized flow models, a single-channel model implies a particular set of phase relations and a special significance to the point where the primitive liquid can coexist with orthopyroxene, but phase relations apparently satisfying these requirements can also appear in liquids produced by two-porosity and continuum flow models, where no single pressure of last equilibration with orthopyroxene exists.

ACKNOWLEDGEMENTS

This paper was motivated by a stimulating conversation with D. H. Green, an invitation to speak at the 2002 Fall AGU Bowen symposium meeting from M. S. Ghiorso and D. Geist, and the hope that M. J. O'Hara will find it intriguing. We acknowledge helpful reviews by C. T. Herzberg and C. C. Lundstrom. It is not our intent to belittle the contributions of experimentalists who have laboured to collect liquidus data over the years in pursuit of multiple saturation points; these experiments have in fact proven essential for calibration of high-pressure melting and fractionation models such as those applied in this study. P.D.A. acknowledges support from the National Science Foundation (OCE-0241716 and EAR-0239513). J.L. acknowledges support from the National Science Foundation (OCE-0084098) and NASA (NAG 5-4649). This is Division of Geological and Planetary Science contribution 8961.

REFERENCES

Aharonov, E., Whitehead, J. A., Kelemen, P. B. & Spiegelman, M. (1995). Channeling instability of upwelling melt in the mantle. *Journal of Geophysical Research* **100**, 20433–20450.

Albarède, F. (1992). How deep do common basaltic magmas form and differentiate? *Journal of Geophysical Research* **97**, 10997–11009.

Asimow, P. D. (1999). A model that reconciles major- and trace-element data from abyssal peridotites. *Earth and Planetary Science Letters* **169**, 303–319.

Asimow, P. D. & Langmuir, C. H. (2003). The importance of water to oceanic mantle melting regimes. *Nature* **421**, 815–820.

Asimow, P. D. & Stolper, E. M. (1999). Steady-state mantle–melt interactions in one dimension: 1. Equilibrium transport and melt focusing. *Journal of Petrology* **40**, 475–494.

Asimow, P. D., Hirschmann, M. M. & Stolper, E. M. (2001). Calculation of peridotite partial melting from thermodynamic models of minerals and melts. IV. Adiabatic decompression and the composition and mean properties of mid-ocean ridge basalts. *Journal of Petrology* **42**, 963–998.

Asimow, P. D., Dixon, J. E. & Langmuir, C. H. (2004). A hydrous melting and fractionation model for mid-ocean ridge basalts: application to the Mid-Atlantic Ridge near the Azores. *Geochemistry, Geophysics, Geosystems* **5**, 10.1029/2003GC000568.

Baker, M. B. & Stolper, E. M. (1994). Determining the composition of high-pressure mantle melts using diamond aggregates. *Geochimica et Cosmochimica Acta* **58**, 2811–2827.

Baker, M. B., Hirschmann, M. M., Ghiorso, M. S. & Stolper, E. M. (1995). Compositions of near-solidus peridotite melts from experiments and thermodynamic calculations. *Nature* **375**, 308–311.

Bender, J. F., Hodges, F. N. & Bence, A. E. (1978). Petrogenesis of basalts from the project FAMOUS area: experimental study from 0 to 15 kbars. *Earth and Planetary Science Letters* **41**, 277–302.

Bowen, N. L. (1928). *The Evolution of the Igneous Rocks*. Princeton, NJ: Princeton University Press.

BVSP (1981). *Basaltic Volcanism on the Terrestrial Planets*. New York: Pergamon.

Engel, A. E., Engel, C. G. & Havens, R. G. (1965). Chemical characteristics of oceanic basalts and the upper mantle. *Geological Society of America Bulletin* **76**, 719–734.

Falloon, T. J. & Green, D. H. (1987). Anhydrous partial melting of MORB pyrolite and other peridotite compositions at 10 kbar: implications for the origin of primitive MORB glasses. *Mineralogy and Petrology* **37**, 181–219.

Falloon, T. J., Green, D. H., Danyushevsky, L. V. & Faul, U. H. (1999). Peridotite melting at 1·0 and 1·5 GPa: an experimental evaluation of techniques using diamond aggregates and mineral mixes for determination of near-solidus melts. *Journal of Petrology* **40**, 1343–1375.

Fujii, T. & Kushiro, I. (1977). Melting relations and viscosity of an abyssal tholeiite. *Carnegie Institution of Washington Yearbook* **76**, 461–464.

Ghiorso, M. S. & Sack, R. O. (1995). Chemical mass transfer in magmatic processes IV. A revised and internally consistent thermodynamic model for the interpolation and extrapolation of liquid–solid equilibria in magmatic systems at elevated temperatures and pressures. *Contributions to Mineralogy and Petrology* **119**, 197–212.

Ghiorso, M. S., Hirschmann, M. M., Reiners, P. W. & Kress, V. C. (2002). The pMELTS: a revision of MELTS for improved calculation of phase relations and major element partitioning related to partial melting of the mantle to 3 GPa. *Geochemistry, Geophysics, Geosystems* **3**, 10.1029/2001GC000217.

Green, D. H. & Ringwood, A. E. (1967). The genesis of basaltic magmas. *Contributions to Mineralogy and Petrology* **15**, 103–190.

Green, D. H., Hibberson, W. O. & Jaques, A. L. (1979). Petrogenesis of mid-ocean ridge basalts. In: McElhinny, M. W. (ed.) *The Earth: its Origin, Structure, and Evolution*. New York: Academic Press, pp. 265–299.

Grove, T. L., Kinzler, R. J. & Bryan, W. B. (1992). Fractionation of mid-ocean ridge basalt (MORB). In: Phipps Morgan, J., Blackman, D. K. & Sinton, J. M. (eds) *Mantle Flow and Melt Generation at Mid-Ocean Ridges. Geophysical Monograph, American Geophysical Union* **71**, 281–310.

Hart, S. R. & Zindler, A. (1986). In search of a bulk-earth composition. *Chemical Geology* **57**, 247–267.

Herzberg, C. T. & O'Hara, M. J. (2002). Plume-associated ultramafic magmas of Phanerozoic age. *Journal of Petrology* **43**, 1857–1883.

Hess, P. C. (1992). Phase equilibria constraints on the origin of ocean floor basalt. In: Phipps Morgan, J., Blackman, D. K. & Sinton, J. M. (eds) *Mantle Flow and Melt Generation at Mid-Ocean Ridges. Geophysical Monograph, American Geophysical Union* **71**, 67–102.

Hirose, K. & Kushiro, I. (1993). Partial melting of dry peridotites at high pressures: determination of compositions of melts segregated from peridotite using aggregates of diamond. *Earth and Planetary Science Letters* **114**, 477–489.

Hirschmann, M. M., Baker, M. B. & Stolper, E. M. (1998*a*). The effect of alkalis on the silica content of mantle-derived melts. *Geochimica et Cosmochimica Acta* **62**, 883–902.

Hirschmann, M. M., Ghiorso, M. S., Wasylenki, L. E., Asimow, P. D. & Stolper, E. M. (1998*b*). Calculation of peridotite partial melting from thermodynamic models of minerals and melts. I. Review of methods and comparison to experiments. *Journal of Petrology* **39**, 1091–1115.

Hirschmann, M. M., Asimow, P. D., Ghiorso, M. S. & Stolper, E. M. (1999*a*). Calculation of peridotite partial melting from thermodynamic models of minerals and melts. III. Controls on isobaric melt production and the effect of water on melt production. *Journal of Petrology* **40**, 831–851.

Hirschmann, M. M., Ghiorso, M. S. & Stolper, E. M. (1999*b*). Calculation of peridotite partial melting from thermodynamic models of minerals and melts. II. Isobaric variations in melts near the solidus and owing to variable source composition. *Journal of Petrology* **40**, 297–313.

Johnson, K. T. M. & Dick, H. J. B. (1992). Open system melting and temporal and spatial variation of peridotite and basalt at the Atlantis II Fracture Zone. *Journal of Geophysical Research* **97**, 9219–9241.

Johnson, K. T. M., Dick, H. J. B. & Shimizu, N. (1990). Melting in the oceanic upper mantle: an ion microprobe study of diopsides in abyssal peridotites. *Journal of Geophysical Research* **95**, 2661–2678.

Kelemen, P. B., Shimizu, N. & Salters, V. J. M. (1995). Extraction of mid-ocean-ridge basalt from the mantle by focused flow of melt in dunite channels. *Nature* **375**, 747–753.

Kelemen, P. B., Hirth, G., Shimizu, N., Spiegelman, M. & Dick, H. J. B. (1997). A review of melt migration processes in the adiabatically upwelling mantle beneath oceanic spreading ridges. *Philosophical Transactions of the Royal Society of London, Series A* **355**, 283–318.

Kinzler, R. J. (1997). Melting of mantle peridotite at pressures approaching the spinel to garnet transition: application to mid-ocean ridge basalt petrogenesis. *Journal of Geophysical Research* **102**, 853–874.

Kinzler, R. J. & Grove, T. L. (1992). Primary magmas of mid-ocean ridge basalts 2. Applications. *Journal of Geophysical Research* **97**, 6907–6926.

Klein, E. M. & Langmuir, C. H. (1987). Global correlations of ocean ridge basalt chemistry with axial depth and crustal thickness. *Journal of Geophysical Research* **92**, 8089–8115.

Kuno, H. (1959). Origin of Cenozoic petrographic provinces of Japan and surrounding areas. *Bulletin of Volcanology, Series 2* **20**, 37–76.

Kushiro, I. & Thompson, R. N. (1972). Origin of some abyssal tholeiites from the mid-Atlantic Ridge. *Carnegie Institution of Washington Yearbook* **71**, 403–406.

Langmuir, C. H., Klein, E. M. & Plank, T. (1992). Petrological systematics of mid-ocean ridge basalts: constraints on melt generation beneath ocean ridges. In: Phipps Morgan, J., Blackman, D. K. & Sinton, J. M. (ed.) *Mantle Flow and Melt Generation at Mid-Ocean Ridges. Geophysical Monograph, American Geophysical Union* **71**, 183–280.

Lehnert, K., Su, Y., Langmuir, C. H., Sarbas, B. & Nohl, U. (2000). A global geochemical database structure for rocks. *Geochemistry, Geophysics, Geosystems* **1**, 1999GC000026.

Longhi, J. (1991). Comparative liquidus equilibria of hypersthene-normative basalts at low-pressure. *American Mineralogist* **76**, 785–800.

Longhi, J. (1992). Origin of green glass magmas by polybaric fractional fusion. *Proceedings in Lunar and Planetary Sciences* **22**, 343–353.

Longhi, J. (2002). Some phase equilibrium systematics of lherzolite melting. *Geochemistry, Geophysics, Geosystems* **3**, 10.1029/2001GC000204.

Longhi, J. (2003). A new view of lunar ferroan anorthosites: post magma ocean petrogenesis. *Journal of Geophysical Research* **108**, 10.1029/2002JE001941.

Longhi, J. (2004). Temporal stability and pressure calibration of barium carbonate and talc/pyrex pressure media in a piston-cylinder apparatus. *American Mineralogist* (in press).

Lundstrom, C. (2000). Models of U-series disequilibria generation in MORB: the effects of two scales of melt porosity. *Physics of the Earth and Planetary Interiors* **121**, 189–204.

Lundstrom, C. C., Gill, J. & Williams, Q. (2000). A geochemically consistent hypothesis for MORB generation. *Chemical Geology* **162**, 105–126.

McKenzie, D. (1984). The generation and compaction of partial melts. *Journal of Petrology* **25**, 713–765.

McKenzie, D. (1985*a*). ^{230}Th–^{238}U disequilibrium and the melting process beneath ridge axes. *Earth and Planetary Science Letters* **72**, 149–157.

McKenzie, D. (1985*b*). The extraction of magma from the crust and mantle. *Earth and Planetary Science Letters* **74**, 81–91.

McKenzie, D. & Bickle, M. J. (1988). The volume and composition of melt generated by extension of the lithosphere. *Journal of Petrology* **29**, 625–679.

McKenzie, D. & O'Nions, R. K. (1991). Partial melt distributions from inversion of rare earth element concentrations. *Journal of Petrology* **32**, 1021–1091.

O'Hara, M. J. (1965). Primary magmas and the origin of basalts. *Scottish Journal of Geology* **1**, 19–40.

O'Hara, M. J. (1968). Are ocean floor basalts primary magmas? *Nature* **220**, 683–686.

Perfit, M. R., Fornari, D. J., Ridley, W. I., Kirk, P. D., Casey, J., Kastens, K. A., Reynolds, J. R., Edwards, M., Desonie, D., Shuster, R. & Paradis, S. (1996). Recent volcanism in the Siqueiros transform fault: picritic basalts and implications for MORB magma genesis. *Earth and Planetary Science Letters* **141**, 91–108.

Plank, T. & Langmuir, C. H. (1992). Effects of the melting regime on the composition of oceanic crust. *Journal of Geophysical Research* **97**, 19749–19770.

Presnall, D. C. & Hoover, J. D. (1987). High pressure phase equilibrium constraints on the origin of mid-ocean ridge basalts. In: Mysen, B. O. (ed.) *Magmatic Processes: Physiochemical Principles. Geochemical Society Special Publication* **1**, 75–89.

Presnall, D. C., Dixon, J. R., O'Donnell, T. H. & Dixon, S. A. (1979). Generation of mid-ocean ridge tholeiites. *Journal of Petrology* **20**, 3–35.

Qin, Z. (1993). Dynamics of melt generation beneath mid-ocean ridge axes; theoretical analysis based on ^{238}U–^{230}Th–^{226}Ra and ^{235}U–^{231}Pa disequilibria. *Geochimica et Cosmochimica Acta* **57**, 1629–1634.

Schwab, B. E. & Johnston, A. D. (2001). Melting systematics of modally variable, compositionally intermediate peridotites and the effects of mineral fertility. *Journal of Petrology* **42**, 1789–1811.

Spiegelman, M. & Kenyon, P. (1992). The requirements for chemical disequilibrium during magma migration. *Earth and Planetary Science Letters* **109**, 611–620.

Stolper, E. M. (1980). A phase diagram for mid-ocean ridge basalts. *Contributions to Mineralogy and Petrology* **74**, 13–27.

Verhoogen, J. (1954). Petrological evidence on temperature distribution in the mantle of the earth. *EOS Transactions, American Geophysical Union* **35**, 85–92.

Walker, D., Shibata, T. & DeLong, S. E. (1979). Abyssal tholeiites from the Oceanographer Fracture Zone. *Contributions to Mineralogy and Petrology* **70**, 111–125.

Walter, M. J. (1998). Melting of garnet peridotite and the origin of komatiite and depleted lithosphere. *Journal of Petrology* **39**, 20–60.

Wendlandt, R. F. & Ridley, W. I. (1994). Melting phase relations of a glassy high-MgO basalt from the Siqueiros Transform Domain, East Pacific Rise (EPR). *EOS Transactions, American Geophysical Union* **75**, 720.

Yoder, H. S. & Tilley, C. E. (1962). Origin of basaltic magmas: experimental study of natural and synthetic rock systems. *Journal of Petrology* **3**, 342–532.